Supplement of Biogeosciences, 18, 6031–6059, 2021
https://doi.org/10.5194/bg-18-6031-2021-supplement

Biogeosciences Open Access EGU

Supplement of

Summertime productivity and carbon export potential in the Weddell Sea, with a focus on the waters adjacent to Larsen C Ice Shelf

Raquel F. Flynn et al.

Correspondence to: Raquel F. Flynn (flyraq001@myuct.ac.za)

This supporting information document provides ancillary methodological detail pertaining to (1) the carbon content of the diatom species identified using light microscopy, (2) the identification of phytoplankton groups via flow cytometry, and (3) estimates of urea uptake for the purposes of computing total nitrogen (N) consumption relative to net primary production (NPP). It additionally includes discussion of (4) multi-variate statistical analyses performed on the data, (5) the relationships of the measured rates of NPP and N uptake to temperature and (6) the upwelling of winter water along Larsen C Ice Shelf. Accompanying the supporting information text are five supplemental figures and two supplemental tables.

Supporting Text

S1. Carbon content of the identified Antarctic diatom species

Light microscopy was used to identify the diatom cells to the lowest taxonomic classification possible. Due to unforeseen circumstances, we were unable to the measure the size and carbon content of individual diatoms. We therefore used the average size (μm) and carbon content (pg C $cell^{-1}$) for the diatom species identified in this study as determined by Leblanc et al. (2012) for the high-latitude Southern Ocean (50 – 70°S) (Table S1).

Table S1. Average carbon content (pg C $cell^{-1}$) assigned to the various diatom species identified via light microscopy, taken from Leblanc et al. (2012) for waters between 50 and 70°S. "–" indicates no available data.

Diatom species	Average carbon content (pg C $cell^{-1}$)
Actinocyclis actinochilus	13575
Amphiprora kufferathi	2115
Amphora sp.	4
Asteromphalus hookeri	1893
Bacteriastrum	2376
Banquisia belgicae	-
Berkeleya rutilans	-
Chaetoceros atlanticus	463
Chaetoceros brevis/neglectus	395
Chaetoceros bulbosa	-
Chaetoceros castracanei	3247
Chaetoceros concavicornis	883
Chaetoceros convolutus	321
Chaetoceros curvatus	388
Chaetoceros debilis	355
Chaetoceros decipiens	1079
Chaetoceros dichaeta	800
Chaetoceros flexuosus	138
Chaetoceros hendeyi	404
Chaetoceros peruvianus	404
Chaetoceros simplex	254
Chaetoceros tortissimus	205
Cocconeis spp	505
Corethron pennatum	317
Coscinodiscus asteromphalus	95958
Coscinodiscus bouvet	22195
Cylindrotheca closterium	300
Dactyliosolen	9039
Entomoneis paludosa	1499
Ephemera planamembranacea	723

Table S1. *continued*

Diatom species	Average carbon content (pg C cell^{-1})
Eucampia antarctica var antarctica	1231
Eucampia antarctica var recta	1231
Fragilariopsis curta	55
Fragilariopsis kerguelensis	283
Fragilariopsis long	243
Fragilariopsis pseudonana	26
Fragilariopsis rhombica	189
Fragilariopsis richerii	243
Fragilariopsis small	26
Gyrosigma sp	5694
Haslea spp	748
Leptocylindrus mediterraneus	1450
Manguinea fusiformis	1114
Membraneis challengeri	12162
Navicula directa	2006
Navicula sp.	1999
Neocalyptrella sp	-
Nitzschia australis	4422
Nitzschia lecontei	4422
Nitzschia medioconstricta	4422
Nitzschia sicula	135
Nitzschia sp.	4422
Nitzschia stellata	4422
Odontella litigosa	4722
Odontella weisflogii	4722
Pinnularia sp	2918
Plagiotropus gaussii	3230
Pleurosigma directum	5050
Proboscia alata	2202
Proboscia inermis	3278
Proboscia sp.	2202
Pseudo-nitzschia sp1	32
Pseudo-nitzschia sp2	32
Pseudo-nitzschia subcurvata	24
Rhizosolenia sp.	3798
Rhizosolenia imbricata	2238
Thalassionema nitzschoides	115
Thalassiosira large	2476
Thalassiosira gracilis	319
Thalassiosira lentignosa	4047
Thalassiosira small	42
Thalassiosira very large	7934
Thalassiothrix antarctica	2456
Trichotoxon reinboldii	4708

S2. Flow cytometric identification of phytoplankton populations

Flow cytometry was used to identify smaller (typically <15 μm) phytoplankton populations at all stations. The size-class of each cell was determined based on forward scatter area (FSC-A) relative to the FSC-A of 2.8 μm and 20 μm beads (Figure S1a). Once categorised as picoplankton (<2.8 μm), nanoplankton (2.8-20 μm) or microplankton (>20 μm), the cells were further subdivided into six populations based on their phycoerythrin (PE) relative to their chlorophyll-a fluorescence (Figure S1b).

Synechococcus (Syn) contain high concentrations of PE and relatively low chlorophyll-a (Marie et al., 2005). We identified two Syn populations, with one population characterized by a lower PE content (Syn 2) than the other (Syn 1; Figure S1b). In contrast to the other phytoplankton groups, the Syn populations were not identified from their size but from their PE vs. chlorophyll-a fluorescence characteristics only. This is because, as Figure S1a shows, the Syn populations were associated with FSC-A values that overlapped with the pico- and nanoplankton size-classes. This signature is an artefact of Syn having a high ratio of photosystem I to photosystem II compared to other phytoplankton, which increases the electron chain activity, leading to an increase in the emission spectrum and low excitation of the Syn populations (Kaprelyants and Kell, 1993; Sunda and Huntsman, 2015).

The picoeukaryotes (PicoEuk), nanoeukaryotes (NanoEuk 1 and 2), and microeukaryotes (MicroEuk) were initially identified from their FSC-A relative to the FSC-A of the 2.8 μm and 20 μm beads (Figure S1a). Additionally, PicoEuk and NanoEuk were characterized by intermediate chlorophyll-a and low PE fluorescence relative to the other phytoplankton groups investigated here (Figure S1b). The PicoEuk and NanoEuk 2 populations fluoresced similarly, with their only discerning factor being size, while the NanoEuk 1 population had relatively higher PE and chlorophyll-a fluorescence than both the PicoEuk and NanoEuk 2 populations. The MicroEuk population had high PE fluorescence and variable chlorophyll-a fluorescence.

To determine the average biovolume of each phytoplankton group, six spherical beads of varying diameters (ranging from 1-15 μm) were run on the flow cytometer. The resulting calibration curve of FSC-A versus volume was used to estimate the biovolume of the PicoEuk, NanoEuk, and MicroEuk populations (Figure S1c; Table S2). Due to the anomalous FSC-A of the Syn populations, the average Syn biovolume was taken from literature (1 μm^3; Kana and Glibert, 1987; Paulsen et al., 2015).

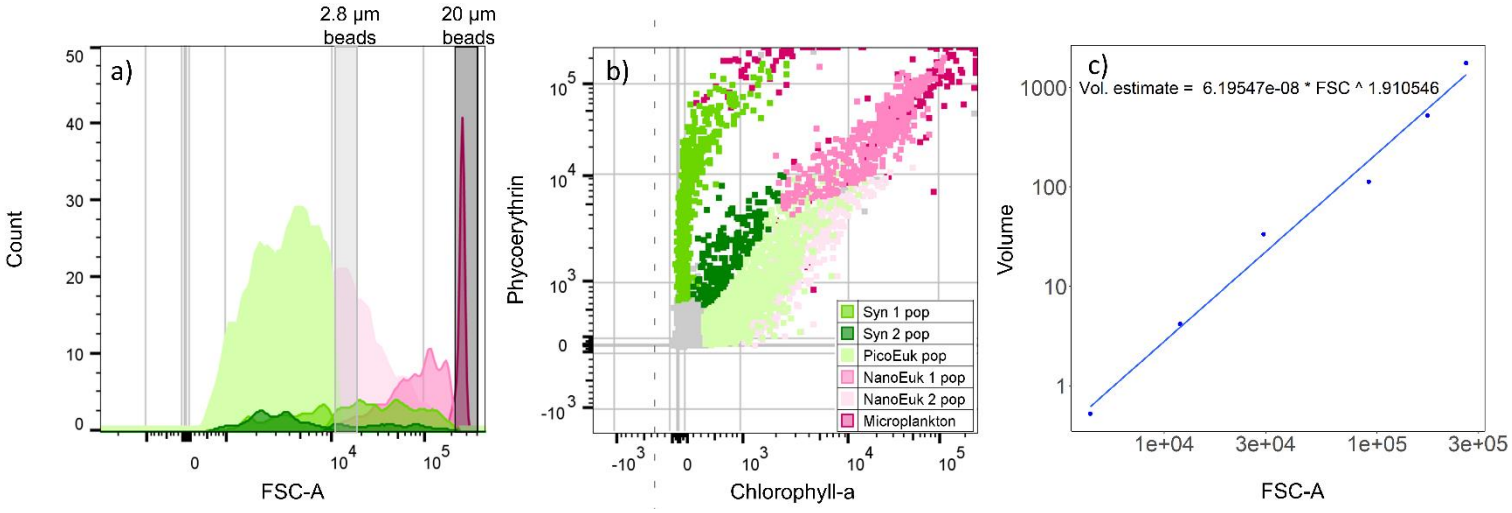

Figure S1. Example (a) histogram of relative cell size as inferred from forward scatter area (FSC-A) and (b) cytogram of phycoerythrin (PE) (i.e., orange) fluorescence versus chlorophyll-a (i.e., red) fluorescence, showing the Weddell Sea populations that were identified using flow cytometry. The populations identified the include: *Synechococcus* (Syn 1 and Syn 2), picoeukaryotes (PicoEuk), nanoeukaryotes (NanoEuk 1 and NanoEuk 2), and microeukaryotes (MicroEuk). Panel (c) shows the calibration curve generated from beads of various sizes that was used to infer the biovolume of the different phytoplankton groups. The grey vertical bars in panel (a) indicate the FSC-A of the 2.8 µm (light grey) and 20 µm beads (dark grey). The grey data in panel (b) show background noise and detritus.

Table S2. Average biovolumes assigned to the various phytoplankton populations identified using flow cytometry. Due to the anomalous FSC-A of the *Synechococcus* populations, the average Syn 1 and Syn 2 biovolumes were set to 1 µm^3 (Kana and Glibert, 1987; Paulsen et al., 2015).

Phytoplankton group	Average biovolume (µm^3)
Synechococcus 1	1
Synechococcus 2	1
Picoeukaryotes	0.7 ± 0.3
Nanoeukaryotes 1	159 ± 69
Nanoeukaryotes 2	52 ± 26
Microeukaryotes	1300 ± 29

S3. Including urea uptake in estimates of total N uptake

If NPP is mainly supported by NO_3^- and NH_4^+ and phytoplankton growth is balanced, then the total N uptake rate (i.e., $\rho N_x = \rho NO_3^- + \rho NH_4^+$) at each station multiplied by the Redfield C:N ratio (6.63) should approximate NPP at that station (e.g., Peng et al., 2018, Mdutyana et al., 2020). For the summertime Weddell Sea, NPP was generally well-accounted for by $\rho NO_3^- + \rho NH_4^+$ only, with N uptake × 6.63 even exceeding NPP at some of the AP and WG stations ($\rho NO_3^- + \rho NH_4^+$ = 142 ± 234% of NPP on average; Figure S2, black symbols). At some of the stations where urea uptake was directly measured (i.e., at LCIS and WG1), ρurea may have been stimulated (i.e., in the cases where total N uptake (= $\rho NO_3^- + \rho NH_4^+ +$ ρurea) × 6.63 exceeds NPP; Figure S2, grey symbols), likely due to the low ambient concentrations of urea-N present in the euphotic zone at the time of sampling (average of 0.2 ± 0.1 μM; Figure 3b and Table 1). Nonetheless, we cannot discount the possibility of urea supporting some fraction of NPP, which has implications for estimating carbon export potential given that urea is a regenerated N form. At the stations where urea uptake was measured (11 out of 19), ρurea accounted for 8 ± 6% of total N uptake. We thus estimated urea uptake at the stations where ρurea was not directly measured by multiplying $\rho NO_3^- + \rho NH_4^+$ by 0.08 (see section 3.3.4; equation 7). If anything, this will lead to an underestimate of the f-ratio and carbon export potential.

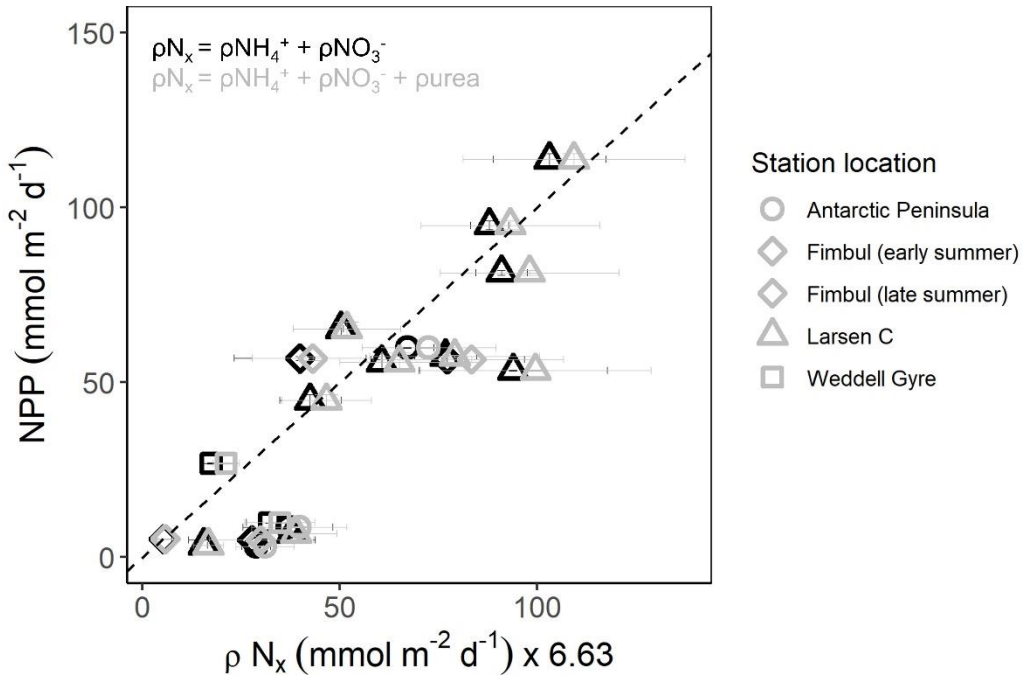

Figure S2. Euphotic zone-integrated rates of NPP and total N uptake (ρN_x) × 6.63. The black symbols represent $\rho N_x = \rho NO_3^- + \rho NH_4^+$ and the grey symbols show $\rho N_x = \rho NO_3^- + \rho NH_4^+ +$ ρurea. The dashed line represents the 1:1 line on which the data points are expected to fall if all N sources supporting NPP are accounted for. Error (± 1 SE) has been propagated according to standard statistical practices.

S4. Multiple dimension statistical analyses

To confirm the relationship of the phytoplankton community to their environment, we performed a Non-metric Multidimensional Scaling (NMDS) and Canonical Correspondence Analysis (CCA) using data from all stations.

NMDS (Figure S3a) is an indirect gradient analysis approach that produces an ordination based on a distance or dissimilarity matrix using Bray-Curtis distance. The NMDS was used to visualise the community composition differences between sites and samples (data were square-root transformed, Bray-Curtis dissimilarity, 999 permutations using Canoco 5). The LCIS and FIS sites were similar to each other and different from the AP and WG sites. AP3 emerged as an outlier, likely due to the very low species diversity and phytoplankton abundance at that station.

The CCA (Figure S3b) summarizes the variation in species composition explained by the environmental variables. Monte Carlo permutation tests (499 permutations) were performed to assess the significance of the canonical axes. The environmental variables considered in the analysis are plotted as arrows originating from the centre of the graph. The origin represents the mean value of each variable, and the arrow represents an increase in the value of that variable. The distance between the symbols approximates the dissimilarity of their species composition as measured by their chi-square distance. Prior to the analysis, co-linearity among possible predictor variables was assessed using variance inflation factors (VIF), with VIFs > 5 deemed co-linear (Zuur et al., 2009, 2010). Therefore, salinity, density, oxygen and PO_4^{3-} were omitted from the analysis. The CCA uses the same species data as plotted in the NMDS but shows the species distribution as constrained by the environmental variables. The AP and WG stations were characterized by higher-than-average temperature (and urea concentrations, although this relationship was less significant). Stations L6, L10, and F3 were characterized by lower-than-average temperature and PAR (consistent with recent sea ice melt and deep MLDs). Station F4 was characterized by higher-than-average PAR and NO_2^- and NO_3^- concentrations, and lower-than-average temperature and NH_4^+ and $Si(OH)_4$ concentrations. The LCIS stations to the left of the centre of Figure S3b (i.e., L1, L2, L4, and L7) were characterized by lower-than-average NO_3^-, NO_2^-, and PAR (likely due to elevated biomass at these stations) and elevated concentrations of NH_4^+ and $Si(OH)_4$.

The NMDS and CCA confirm that the LCIS stations were statistically different from the AP and WG stations, as indicated by the observed variability in the Si:N:P depletion ratios and the dominant phytoplankton groups (i.e., *P. antarctica* at LCIS and diatoms at the AP and WG stations) between the station locations. The LCIS stations were generally characterized by elevated NH_4^+ and urea concentrations (Figures 3a and b), the result of increased heterotrophy and an upregulated microbial loop, and high $Si(OH)_4$ concentrations (Figure 3e), likely the result of low $Si(OH)_4$ uptake by a phytoplankton community consisting of a low abundance of diatoms (Figure 9). Furthermore, the lowest

Si:N and highest N:P depletion ratios were observed at LCIS (consistent with *P. antarctica* dominance), while the highest Si:N and lowest N:P depletion ratios occurred at FIS and in the WG (consistent with diatom dominance; Figures 4 and 11; Table 1). The variability in phytoplankton community composition appears to have been largely driven by the mechanisms controlling water column stratification, as discussed at length in the main text.

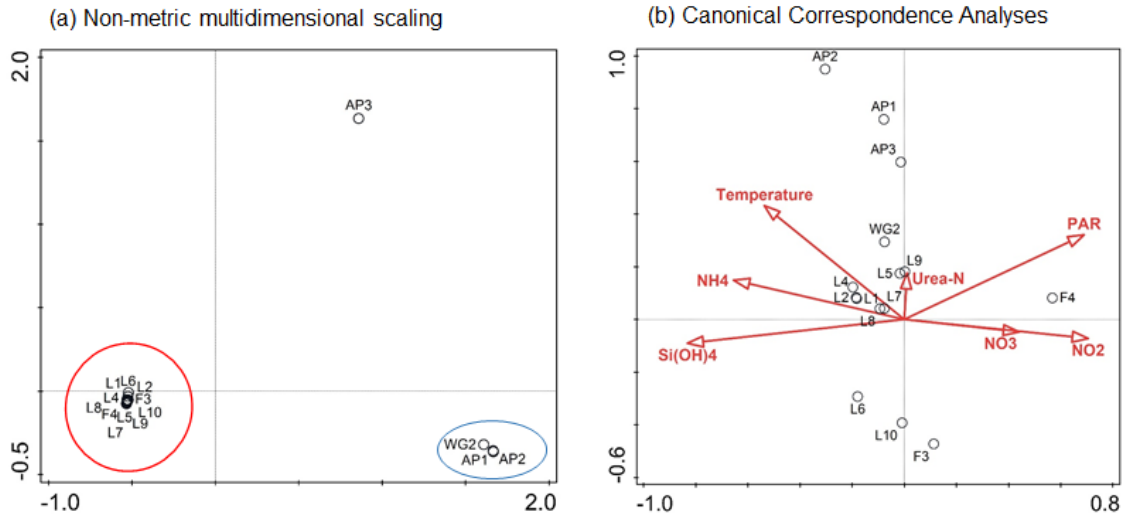

Figure S3: (a) NMDS analysis of the variability in phytoplankton community composition among stations and (b) CCA ordination of phytoplankton species constrained by environmental variables, visualized as a biplot with sampling stations labeled (see Figure 1 for station positions).

S5. Apparent effect of temperature on NPP and N uptake

The euphotic zone-averaged rates of NPP and N uptake (μM d^{-1}) generally increased with increasing sea surface temperature (SST) across our study region (Figures S4a-d). Antarctic phytoplankton growth rates are known to be temperature-sensitive, with very low temperatures limiting cellular metabolic rates (Neori and Holm-Hansen, 1982). However, while the transport rates measured here were positively correlated with SST, the specific rates of carbon fixation and N uptake (d^{-1}; both proxies for growth rate) showed no such relationship (Figure S4e), suggesting that the phytoplankton community was adapted to the low *in situ* temperatures (Bracher et al., 1999). The observed increase in NPP and N uptake with SST can instead be explained by the observed increase in biomass (i.e., POC and PON) with SST (Figure S4f; because transport rate = specific rate × biomass). Given this observation, we propose that SST can be used as a measure of time, particularly at LCIS where the stations are very close together, with warmer SSTs indicating "older" surface waters and cooler SST evincing recently upwelled WW. The higher rates of NPP and N uptake in the warm surface waters can be attributed to phytoplankton having experienced favourable growth conditions for an extended period such that biomass has accumulated, while in cold, newly-upwelled waters, little phytoplankton growth has occurred.

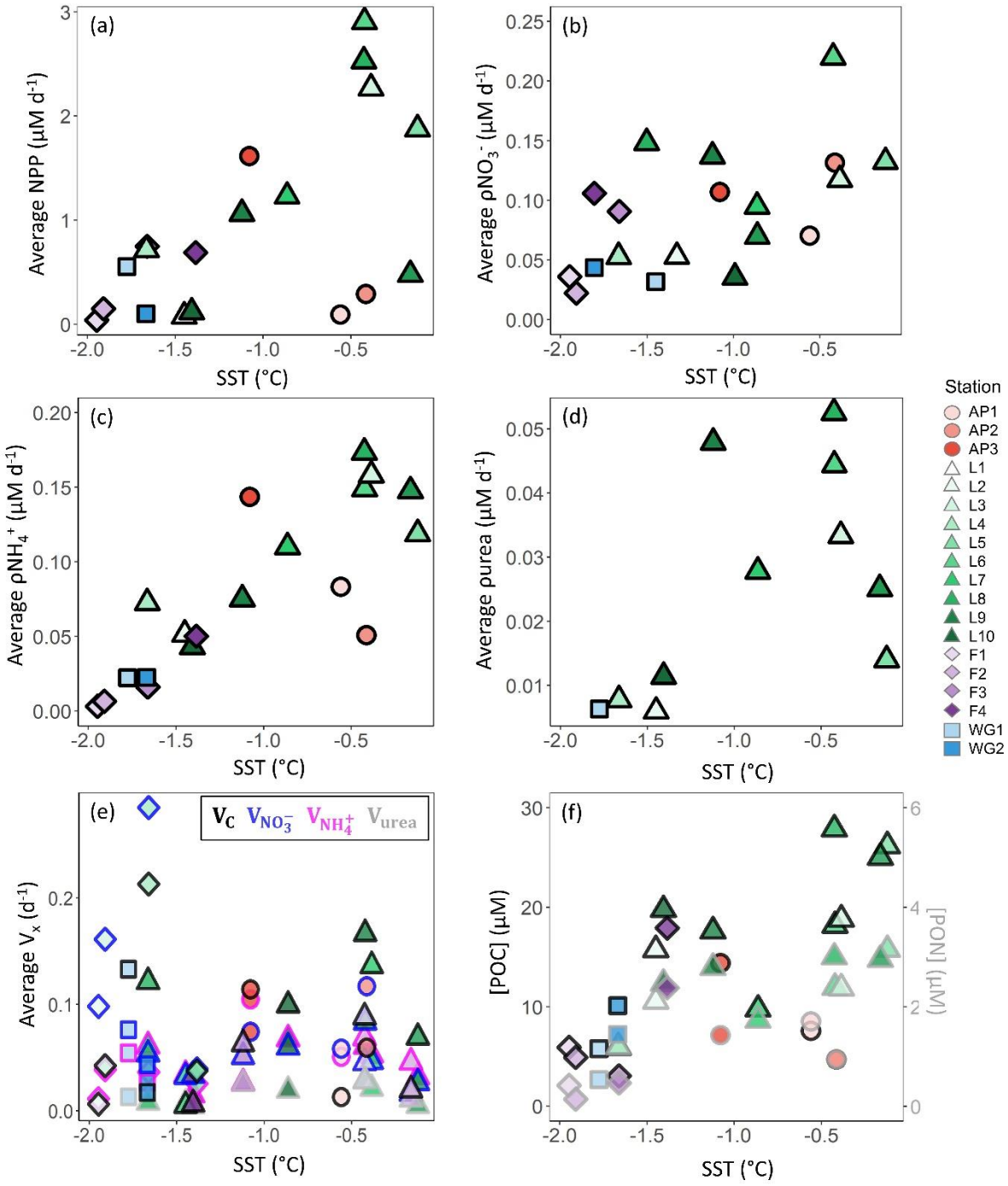

Figure S4. Average euphotic zone rates of (a) net primary production (NPP), (b) NO_3^- uptake (ρNO_3^-), (c) NH_4^+ uptake (ρNH_4^+), and (d) urea uptake (ρurea) as a function of sea surface temperature (SST), as well as the (e) specific rates of NPP, NO_3^-, NH_4^+, and urea uptake (V_X) and (f) concentrations of POC (black outline; left y-axis) and PON (grey outline; right y-axis) versus SST. The symbol outline colours in panel (e) denote the specific uptake rates of carbon (black), NO_3^- (blue), NH_4^+ (pink), and urea (grey).

S5. Upwelling of Winter Water along LCIS

At LCIS, localised "pockets" of cool, saline surface waters were present along the ice shelf front (Figure S5a-b). This is due to the upwelling of winter water (WW; the source water mass to the surface) at the ice shelf. From the oxygen content of these surface waters, we deduce that these waters were recently upwelled – their oxygen concentrations were low (and below saturation) compared to the other stations (Figure S5c-d), such that these cool, saline surface waters cannot be attributed to another physical process (e.g., sea-ice melt). Furthermore, the oxygen concentrations in the mixed layer at these stations were contiguous with underlying WW, while the other stations at LCIS (i.e., the "non-upwelling" stations) exhibited an increase in oxygen concentration towards the surface (Figure S5d) due to gas exchange with the atmosphere and phytoplankton and sea-ice algae growth.

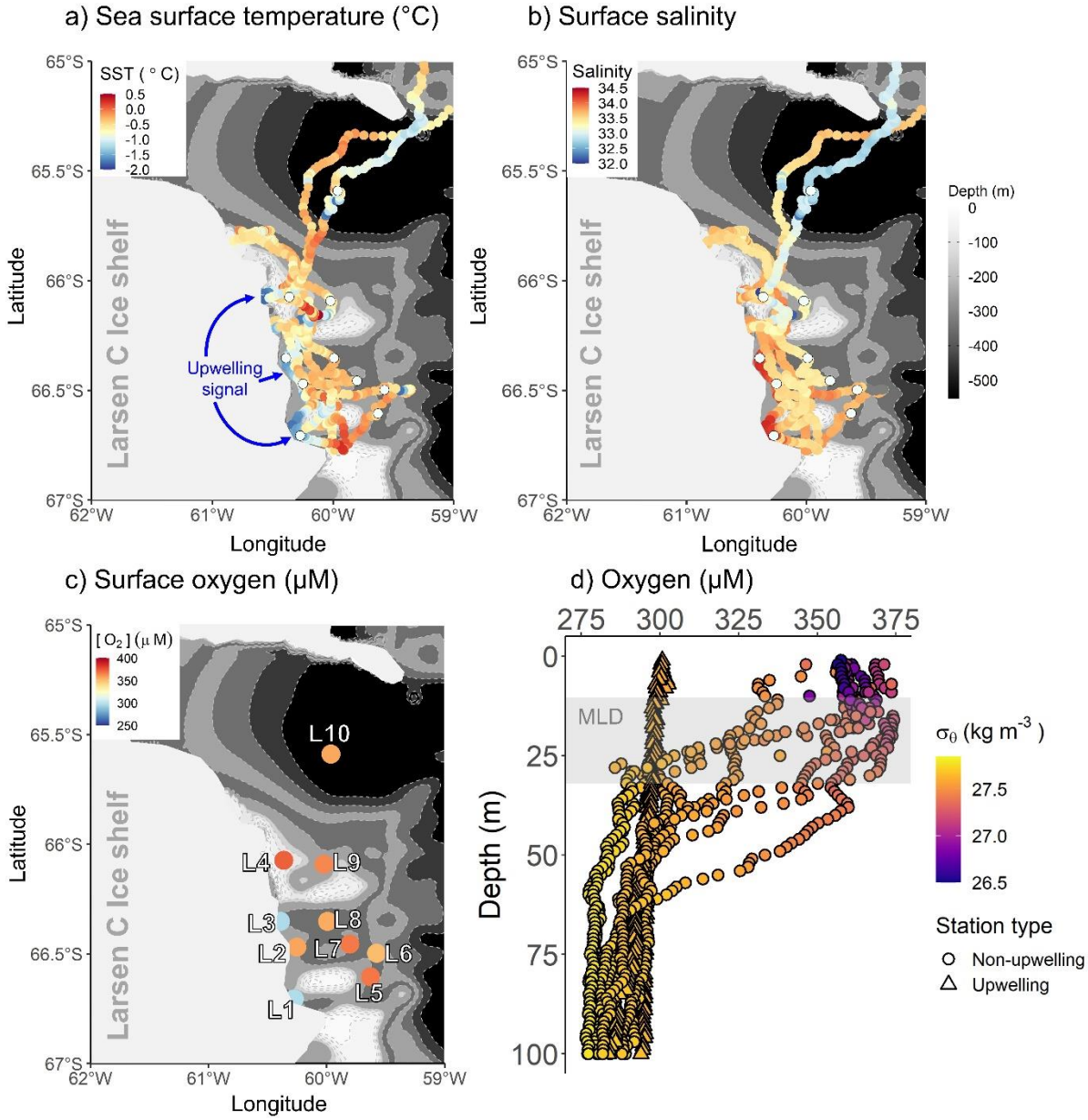

Figure S5. Maps of (a) SST, (b) sea surface salinity, and (c) surface oxygen concentrations and (d)

depth profiles of oxygen concentrations in the region of LCIS at the time of sampling. SST and salinity data were acquired from the underway (~7 m inflow) ferrybox, while the oxygen concentrations were measured via the oxygen sensor on the CTD profiler, calibrated against discrete seawater samples measured for dissolved oxygen by Winkler titration (Carpenter, 1965; Grasshoff et al., 1983; Hutchinson et al., 2020). The symbols in panel (d) are coloured by potential density (σ_θ), with the circles indicating the "non-upwelling" stations and the triangles the upwelling stations. The grey box in panel (d) indicates the average mixed layer depth (MLD) ± 1 SD across the stations at LCIS (n=10). The bathymetry data in panels (a-c) were taken from ETOPO1 (NOAA National Geophysical Data Center, 2009).

Supplemental references cited:

Bracher, A. U., Kroon, B. M. A., and Lucas, M. I.: Primary production, physiological state and composition of phytoplankton in the Atlantic sector of the Southern Ocean, Mar. Ecol. Prog. Ser., 190, 1–16, https://doi.org/10.3354/meps190001, 1999.

Carpenter, J.: The Chesapeake Bay Institute technique for the Winkler dissolved oxygen method., Limnol. Oceanogr., 10, 141–143, 1965.

Grasshoff, K., Kremling, K., and Ehrhard, M.: Methods of seawater analysis, Florida: Verlag Chemia, 1983.

Hutchinson, K., Deshayes, J., Sallee, J. B., Dowdeswell, J. A., de Lavergne, C., Ansorge, I., Luyt, H., Henry, T., and Fawcett, S. E.: Water Mass Characteristics and Distribution Adjacent to Larsen C Ice Shelf, Antarctica, J. Geophys. Res. Ocean., 125, 0–2, https://doi.org/10.1029/2019JC015855, 2020.

Kana, T. M. and Glibert, P. M.: Effect of irradiances up to 2000 μE m-2 s-1 on marine Synechococcus WH7803-I. Growth, pigmentation, and cell composition, Deep Sea Res. Part A, Oceanogr. Res. Pap., 34, 479–495, https://doi.org/10.1016/0198-0149(87)90001-X, 1987.

Kaprelyants, A. S. and Kell, D. B.: Dormancy in stationary-phase cultures of Micrococcus luteus: flow cytometric analysis of starvation and resuscitation, 1Applied Environ. Microbiol., 59, 3187–3196, 1993.

Leblanc, K., Arístegui, J., Armand, L., Assmy, P., Beker, B., Bode, A., Breton, E., Cornet, V., Gibson, J., Gosselin, M. P., Kopczynska, E., Marshall, H., Peloquin, J., Piontkovski, S., Poulton, A. J., Quéguiner, B., Schiebel, R., Shipe, R., Stefels, J., Van Leeuwe, M. A., Varela, M., Widdicombe, C., and Yallop, M.: A global diatom database- A bundance, biovolume and biomass in the world ocean, Earth Syst. Sci. Data, 4, 149–165, https://doi.org/10.5194/ESSD-4-149-2012, 2012.

Marie, D., Pierre, U., Curie, M., Simon, N., and Vaulot, D.: Algae Culturing Techniques Chapter 17: Phytoplankton Cell Counting by Flow Cytometry, 1–15, 2005.

Mdutyana, M., Thomalla, S. J., Philibert, R., Ward, B. B., and Fawcett, S. E.: The Seasonal Cycle of Nitrogen Uptake and Nitrification in the Atlantic Sector of the Southern Ocean, Global Biogeochem.

Cycles, 34, 1–29, https://doi.org/10.1029/2019GB006363, 2020.

Neori, A. and Holm-Hansen, O.: Effect of temperature on rate of photosynthesis in Antarctic phytoplankton, Polar Biol. 1982 11, 1, 33–38, https://doi.org/10.1007/BF00568752, 1982.

Paulsen, M. L., Riisgaard, K., Thingstad, T. F., John, M. S., and Nielsen, T. G.: Winter-spring transition in the subarctic Atlantic: Microbial response to deep mixing and pre-bloom production., Aquat. Microb. Ecol., 76, 49–49, 2015.

Peng, X., Fawcett, S. E., Van Oostende, N., Wolf, M. J., Marconi, D., Sigman, D. M., and Ward, B. B.: Nitrogen uptake and nitrification in the subarctic North Atlantic Ocean, https://doi.org/10.1002/lno.10784, 2018.

Sunda, W. G. and Huntsman, S. A.: High iron requirement for growth, photosynthesis, and low-light acclimation in the coastal cyanobacterium Synechococcus bacillaris, Front. Microbiol., 6, 561, 2015.

Zuur, A. F., Ieno, E. N., Walker, N. J., Saveliev, A. A., and Smith, G. M.: Introduction, 1–10, https://doi.org/10.1007/978-0-387-87458-6_1, 2009.

Zuur, A. F., Ieno, E. N., and Elphick, C. S.: A protocol for data exploration to avoid common statistical problems, Methods Ecol. Evol., 1, 3–14, https://doi.org/10.1111/J.2041-210X.2009.00001.X, 2010.